JOURNAL OF MATERIALS SCIENCE **38** (2003) 2747–2754

The viscoelastic behavior of β-In_3Sn and the nature of the high-temperature background

K. M. McMILLAN
Department of Physics, Bradley University, Peoria, IL 61615, USA; Program in Mechanics and Materials, University of Wisconsin–Madison, Madison, WI 53706, USA

R. S. LAKES*
Department of Engineering Physics, Department of Biomedical Engineering, Program in Mechanics and Materials, University of Wisconsin–Madison, Madison, WI 53706, USA
E-mail: lakes@engr.wisc.edu

R. F. COOPER
Department of Materials Science and Engineering, Program in Mechanics and Materials, University of Wisconsin–Madison, Madison, WI 53706, USA

T. LEE†
Department of Biomedical Engineering, Program in Mechanics and Materials, University of Wisconsin—Madison, Madison, WI 53706, USA

The damping behavior in torsion of single phase β-In_3Sn has been evaluated at room temperature over a broad range of frequencies (10^{-4} to 10^3 Hz) and as a function of various mechanical and thermal treatments. The results are consistent with a model for the power-law ($\tan\delta \propto f^{-n}$), high-temperature-background absorption being effected by diffusional processes on grain and, particularly, on subgrain boundaries. The results are compared/contrasted with those for damping in single-phase γ-$InSn_4$ and in the two-phase β-γ eutectic. Failure of the eutectic material to follow a composite model for damping, combined with a thermal aging effect that lowers damping only for certain frequencies, shows that the boundary-based absorption model for the high-temperature background applies, too, to phase boundaries.

1. Introduction

1.1. Viscoelasticity and the pursuit of high-stiffness/high-damping structural materials

Viscoelastic materials for structural applications can combine the suppression of mechanical vibration for noise control with structural stability [1]. One may use a material's intrinsic damping capability to reduce unwanted vibration in structures without the use of external dampers [2]. At the same time, it is desirable to use stiff materials in a structural role. Stiff materials generally have low damping capabilities, however (a loss tangent, $\tan\delta$, of 10^{-3} or less) [3]. Polymers, on the other hand, have a loss tangent between 0.1 to 1 or more [4], but they tend to be compliant. Therefore, a layer of polymer is often cemented to a layer of stiff material to attempt to increase damping while retaining stiffness [3]. These polymer layers are quite temperature sensitive and may experience problems in aggressive environments. There is, consequently, an interest in developing crystalline materials with high stiffness and an intrinsically high loss tangent to be used in damping vibrations in structures and vehicles, especially in situations where polymer layers have proven ineffective [4]. Although the study of relaxation mechanisms has been conducted for some years, attempts at the intentional design of materials with high loss based on known mechanisms is relatively recent, and the field is embryonic at this stage. For example, the thermoelastic mechanism has been investigated by Bishop and Kinra [5] with the aim of developing composites with enhanced damping. In thermoelastic damping, dissipation of mechanical energy occurs as a result of heat flow due to the coupling of thermal expansion [6]. Thermoelastic losses in most common materials are small, but in a composite with zinc inclusions, a maximum $\tan\delta$ on the order of 0.01 could be achieved.

Our efforts have emphasized accessing damping associated with the "high-temperature background," specifically through microstructural control to manipulate the value of $\tan\delta$ associated with a given temperature and frequency. Phenomenologically, the high-temperature background refers to damping

*Author to whom all correspondence should be addressed.
†Present address Orthopedic Biomechanics Laboratory, Beth Israel Deaconess Medical Center, Boston, MA, USA.

observed in crystalline materials at high homologous temperature, e.g., $T_h \equiv T/T_{solidus} \geq 0.5$, and is associated with a broad-frequency-range power-law spectrum for damping, i.e., $\tan \delta \propto f^{-n}$ (where f is frequency). The physics of this high-T background damping are poorly understood; we report here observations and interpretations that contribute to a description of the phenomenon.

1.2. High-temperature background

Early interpretation of the physics of the high-temperature background is summarized in the work of Nowick and Berry [7]. The high-T background depends on structure; for generalizations, one can defend that (1) it is smaller in single crystals than in polycrystals; (2) it is smaller in coarse-grained polycrystals than in fine-grained polycrystals; (3) it is enhanced in deformed and partially-recovered or polygonized samples; and (4) it is reduced by annealing treatments at successively higher temperatures. It is commonly held that the background is caused by a combination of thermally-activated dislocation mechanisms, such as drag between dislocations and point defects, e.g., the model of Schoeck *et al.* [8]. Their result is

$$\tan \delta = \frac{Q}{[2\pi f \exp(U_o/kT)]^n}, \qquad (1)$$

where U_o is the activation energy of the rate-controlling process, kT has its usual meaning and Q and n are constants. Nevertheless, Schoeck *et al.* were not able to correctly predict the power-law exponent n. Experimentally, n falls somewhere between 0.2 and 0.4.

The power-law relationship expressed in Equation 1 is manifest physically as a continuous distribution of material compliances (e.g. [9]). In the dynamic response of polymers, such a relationship is easily contemplated: relaxations are associated with motions of differing lengths of the nominally continuous polymer chains; these integrate to produce the power-law damping. The general approach to the high-T background in crystalline solids, e.g., as presented in the model referenced above, has followed a similar logic: a distribution of length scales in dislocation rheology is postulated. This approach is problematic, however: physical metallurgy constraints suggest that it is difficult to cite the required length scales that must vary some two orders of magnitude or more. Strain-energy-gradient and chemical-diffusion-gradient driving forces tend to make relatively homogeneous the distribution of dislocation pinning sources like precipitates or substitutional or interstitial point defects. For bcc metals and compounds and all ceramics, the intrinsic resistance of the lattice to the glide of dislocations (the Peierl's stress) suggests that glide motion is limited by the nucleation of kinks. This logic suggests, then, that most such mechanisms should produce specific absorption peaks, whose characteristic frequency and width are sensitive to temperature, instead of the power-law "band".

Recent data on the high-temperature damping behavior of polycrystalline, ferromagnesian olivine ($[Mg_{0.92}Fe_{0.08}]_2SiO_4$) [10] illustrate the conundrum. Specimens were prepared with such a fine and uniform grain size ($d \approx 3$ μm) that, for both the stress used in hot-press fabrication of the aggregates as well as in the mechanical testing, no lattice dislocations are nucleated or present. Thus, the experiments probed uniquely the role, in an aggregate having a Newtonian (chemical-diffusion-effected) steady-state viscosity, of high-angle grain boundaries in damping. Despite there being absolutely no significant variation whatsoever in any microstructural feature, the measured damping displayed nevertheless the power-law behavior, with $\tan \delta \propto f^{-0.35}$ over the frequency range explored (10^{-3}–10^{0} Hz). Further, the damping response could be predicted very accurately from the transient (anelastic) response in unidirectional creep, where the anelastic strain was seen to vary as $\varepsilon_a \propto t^m$, where $1/3 \leq m \leq 1/2$ (cf. the Andrade model for viscoelastic rheology [11]).

In this system, the anelasticity and subsequent damping response is easily understood (and modeled all-but-exactly) as resulting from chemical diffusion in a diminishing potential (cf. [12]): assuming inviscid grain boundaries, far-field loading with any shear components produces stress concentrations at grain triple junctions; in the fine-grained material, this excess strain energy must be dissipated by chemical diffusion either through the grains (i.e., the process described by Nabarro [13] and by Herring [14]) or through the grain boundaries (i.e., the process described by Coble [15]), leading to a distribution of traction that allows for a steady-state diffusion flux (steady-state creep rate). In this situation, "free" lattice dislocations clearly play no role in the high-T background damping whatsoever.

Such an understanding allows straightforward extrapolation to larger grain size. What is discovered, though, is that the data for $d \approx 3$ μm olivine predict a tan δ for a 300 μm grain size that is significantly lower (an order of magnitude at 1200°C and 1 Hz) than that measured for a ~1 cm-scale olivine single crystal that was first plastically deformed (via the motion of lattice dislocations) to steady state at a differential stress of 20 MPa [16]. One can correlate the results, however, by realizing that, in the steady-state dislocation rheology, the single crystal must develop a polygonized microstructure, that is, there is developed a three-dimensional network of low-angle subgrain boundaries whose mean spacing is set by the level of differential stress [17, 18]. For olivine, a 20 MPa differential stress creates a mean subgrain boundary spacing of ~20 μm; intriguingly, extrapolation of the 3-μm polycrystalline data to a grain size of 20 μm matches beautifully with the single-crystal data.

Diffusional dissipation of mechanical energy predicated on grain- or subgrain-scale potentials for chemical diffusion clearly is suggested as a (the?) physical mechanism for the high-T background in non-fcc metals and in crystalline ceramics. It is supported, too, by studies seeking to isolate the grain boundary/subgrain boundary absorption peak (i.e., as first described by Kê

[19] and more recently illustrated by the works of Yan and Kê [20], Rivière and Gadaud [21] and Kong *et al.* [22]); given the dislocation structure of both high- and low-angle grain boundaries, one can anticipate the existence and evolution with annealing of an absorption peak at a frequency related to the exact boundary structure (in turn, functions of the slip systems available and activated by the differential stress in creep). For isothermal conditions, then, one further anticipates the behavior of the subgrain boundaries to be that envisioned by Raj [12] and Raj and Ashby [23]: inviscid sliding producing triple-junction loading at frequencies lower than the boundary peak; elastic triple junction loading at frequencies above the boundary peak. Note, too, this perspective on the high-T background absorption behavior is consistent with models attempting to formulate a microstructural basis for a mechanical equation of state [24].

The experimental effort reported here represents initial steps towards the quantification of the impact of high- and low-angle grain boundaries, not on specific peaks in attenuation, but rather on the high-T background. A hierarchical study is required, that is, one must first attempt to effect quantifiable changes in boundary structure and spatial distribution (density) in a single phase system; beyond this, one can begin to address the impact of solid-state phase boundaries, e.g., as exist in eutectic structures. To this end, we here concentrate on the absorption behavior of single-phase β-In_3Sn as affected by different processing conditions designed to effect different internal structures; further, we compare these results to measurements made on the eutectic β-In_3Sn/γ-$InSn_4$ (β-γ). (The absorption behavior of the β-γ eutectic was examined earlier, in view of its immediate applications as a solder and its potential as a material that simultaneously displays both a high modulus and high damping [4].)

β-In_3Sn is not an intermetallic compound but is rather an endothermic solid solution of wide compositional variation [25] that has the same crystal structure as pure In. This structure, in its fundamental form, is described as body-centered tetragonal (bct: *Pearson tI*2; space group $I4/mmm$, number 139). The c/a ratio of the lattice, nominally 1.24 (i.e., significantly less than $\sqrt{2}$), is sufficiently small such that the structure's description as a face-centered tetragonal (fct) structure ($F4/mmm$, with $a' = b' = \sqrt{2}a$ and $c' = c$; $c'/a' = 0.90$) is important in the description of dislocation properties: the most prevalent slip system is anticipated as 1/2[101];(111) based on the fct structure. One determines that not all Burgers vectors (**b**) on this plane are equivalent: for example, $\mathbf{b} = 1/2[110]_{\text{fct}}$ has an energy some 11% greater than $1/2[101]_{\text{fct}}$; as such, dislocation-effected flow at low differential stress is anticipated as somewhat restricted due to a reduced number of active slip systems.

In the experimental work described below, specimens of a single-phase β composition are subjected to various process conditions and then their room-temperature absorption behavior measured over a wide range of frequencies. The process conditions include (1) a high-rate, high-strain plastic deformation (referred to here as "pressing"), (2) pressing followed by elevated-temperature static annealing, and (3) tensile creep to relatively large strain following pressing and annealing. Pressing should produce a high density of "free" dislocations and increase hardness. Subsequent static annealing of a specimen is expected to lower the free dislocation density, affect the density of dislocation arrays (i.e. subgrain boundary spacing and lattice misorientation), and, perhaps, to increase grain size. Steady-state creep can be used to engineer a specific density of dislocations and subgrain boundaries [17, 18].

2. Experimental approach

2.1. Specimen preparation

Ingots of β-In_3Sn, of composition 80 at.% In–20 at.% Sn, were cast in glass tubing (Corning Code 7740, Pyrex^{TM}) under a vacuum of 10^{-3} atm. X-ray diffraction results compared with the JCPDF database confirmed the composition was single-phase β. Further preparation included pressing—uniaxial compressive deformation—to 63% strain. Specimens subsequently annealed were done so at 389 K (93% of the solidus temperature) for ~3.5 h (one specimen was annealed for ~40 h). Annealed specimens that also received a creep treatment were subjected to tensile loading: one specimen at an initial stress of 2.04 MPa ($4 \times 10^{-4}\ G$, where G is the unrelaxed shear modulus, see below; the specimen was crept to 30% strain after 5–10 h), the other at an initial stress of 1.35 MPa ($2.6 \times 10^{-4}\ G$; crept to 19% strain in 50 h).

All specimens for oscillatory load testing were rectangular, and the shapes were prepared with a low-speed diamond saw. Specimen dimensions were as follows: as-cast specimen, $2.1 \times 3.0 \times 23.4$ mm; pressed sample, $2.43 \times 2.68 \times 25.91$ mm; pressed-and-annealed specimen, $2.42 \times 2.69 \times 25.1$ mm. The specimen crept at the lower stress has dimensions $2.18 \times 2.22 \times 20.16$ mm for the oscillating tests (some length was lost in its removal from the creep apparatus). The higher differential stress induced an unstable creep that cause some minor strain instabilities. As such, the specimen cross-section dimensions were not uniform: there were two points where the sample was very thin. At the regions of more homogeneous deformation, however, cross-section dimensions were approximately 2.4×3.2 mm. This sample was tested under oscillatory load of various frequencies at a length 20.52 mm, the length again representing some loss of specimen in its removal from the creep apparatus.

2.2. Stiffness/damping tests and microscopy

Viscoelastic testing was performed using the modified [3, 26] broadband viscoelastic spectroscopy (BVS) apparatus [27] shown in Fig. 1. The instrument is capable of providing a wide range of frequencies in an isothermal environment which is particularly useful when studying specimens that are thermorheologically complex. The apparatus was used for studies in torsion in sub-resonant and resonant dynamic oscillation on

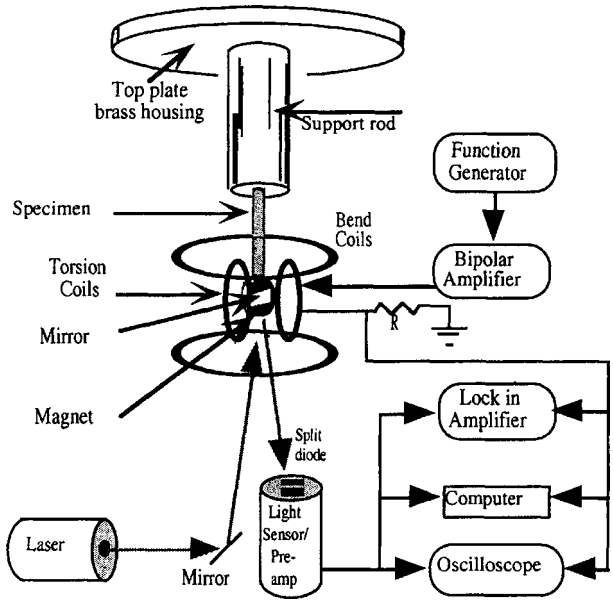

Figure 1 Broadband Viscoelastic Spectroscopy (BVS) apparatus (schematic; after [26]).

β-In_3Sn. The full range of capabilities of the BVS instrument is demonstrated by the β-γ eutectic and single-phase γ-$InSn_4$ studies [3], compared with β below.

Dynamic experiments were conducted by applying a sinusoidal voltage from a digital function generator to the Helmholtz coil. A cyanoacrylate cement was used to bind the top of specimens to a support rod and the bottom to a high magnetic intensity neodymium iron boron magnet. A mirror of appropriate size was attached to the magnet. The coil imposed a magnetic field on the permanent magnet and transmitted an axial torque on the specimen. The angular displacement of the specimen was measured using laser light reflected from a mirror mounted on the magnet to a split-diode light detector. Torque was inferred from the Helmholtz coil current. Torque calculations were supported by calibrations using the well-characterized Al alloy type 6061 ($E = 68.9$ GPa, $G = 25.9$ GPa, $\tan\delta \approx 3.6 \times 10^{-6}$) [28]. Input and output voltages were recorded using a digital data acquisition system containing a Macintosh IIci computer and LabVIEW interface hardware and software. Near resonances, signals were measured using a digitizing oscilloscope. At low frequency, the phase angle between torque and angular displacement was determined from the width of elliptic Lissajous figures. At frequencies above 0.01 Hz, phase angle was determined using a lock-in amplifier (SRS 850) with claimed phase resolution of 0.001 degree. The frequency range was segmented into regions less than 1 Hz and greater than 1 Hz since the wide frequency range necessitated different time constant settings [29].

Data reduction was conducted as follows. For frequencies sufficiently below the first natural frequency, torsional stiffness is given by $|G^*| \approx K\frac{|M^*|L}{\theta}$ and loss by $\tan\delta \approx \tan\Phi$, in which K is a geometrical factor for torsion of a rectangular section and Φ is the observed phase difference between stress and displacement. At the resonance angular frequencies ω_o in torsion, damping was calculated using the width $\Delta\omega$ at half maximum of the curve of dynamic structural compliance θ/M^* as follows:

$$\tan\delta \approx \frac{1}{\sqrt{3}}\frac{\Delta\omega}{\omega_o}. \qquad (2)$$

Strains were calculated at 1 Hz for each of the specimens. The maximum values occurred in the sample crept at the smaller of two strains; in torsion, the maximum strain was 9.8×10^{-7}. Lissajous figures were examined to discriminate between linear and nonlinear behavior. All studies were confirmed in the linear range.

β specimens of all preparations (including post-oscillatory testing) were examined in optical microscopy, both to characterize grain size as well as to discern features of the as-processed and –deformed microstructures. Each β sample was cleaved using a microtome: specimens were first embedded in JB-4 resin (Polysciences, Inc.) using standard molds and an aluminum chuck; the embedded samples were placed in a Sorvall/DuPont JB-4 microtome, and a clean block face was cut using 9.5-mm glass knives. The knives were replaced frequently to achieve a clean surface. A final 5-μm-thick section was taken with a new glass knife to avoid knife marks and the related "smearing" of the specimen.

In order to image grain boundaries, β samples were etched with 70% nitric acid. An optimal etch time for each specimen type was not found. Each started with a ten-second etch and the procedure was repeated for five seconds as needed. After each etching, specimens were thoroughly rinsed with methanol, then quickly dried. An Olympus BH-4 petrographic microscope was used in reflection mode for subsequent examination; images were recorded digitally (Pixera PVC 100C camera).

3. Experimental results and comment

Viscoelastic properties of cast β-In_3Sn in torsion are shown in Fig. 2; also shown for comparison are torsional properties of single-phase γ-$InSn_4$ and β-γ

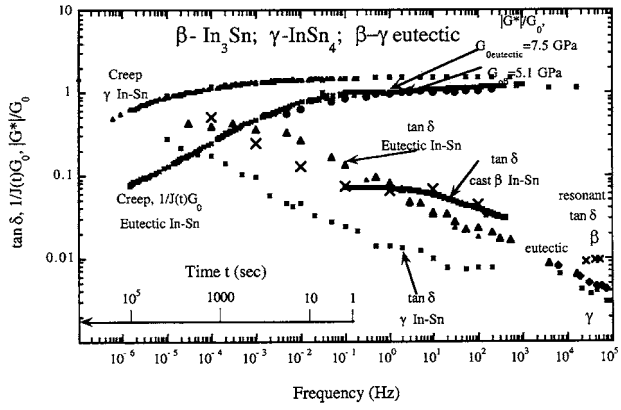

Figure 2 Torsional viscoelastic response ($\tan\delta$) and normalized complex shear modulus ($|G^*|$) as functions of frequency, and creep compliance (J(t)) as a function of time, for β-In_3Sn, γ-$InSn_4$ and the β-γ eutectic, all in the as-cast condition and at room temperature. One sees that the "standard," power-law, high-T background behavior holds for both single-phase β and γ materials at low frequency ($n \sim 0.3$; cf. Equation 1); both β and γ deviate from this behavior at increasing frequency ($\sim 10^{-1}$ Hz for β; ~ 1 Hz for γ) The time scale for creep (inset) is related to the frequency scale by $2\pi f = 1/t$.

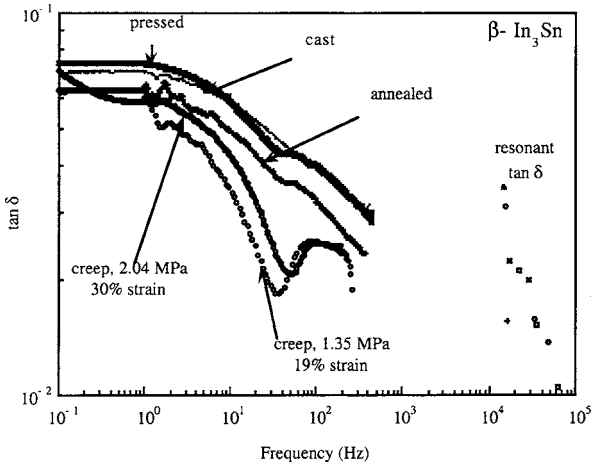

Figure 3 Room-temperature, torsional viscoelastic response of β-In_3Sn specimens as functions of processing conditions. The processing followed a hierarchy of as-cast; cast + pressed (high-rate, high-strain deformation); cast + pressed + annealed; cast + pressed + annealed + creep. One sees a significant effect of the creep treatment: despite an increase in lattice dislocation density due to the tensile deformation, the torsional damping actually decreases. Too, an absorption peak is enhanced at $\sim 10^2$ Hz. Both results suggest an important—perhaps dominant—role of low-angle boundaries in effecting the high-T background absorption.

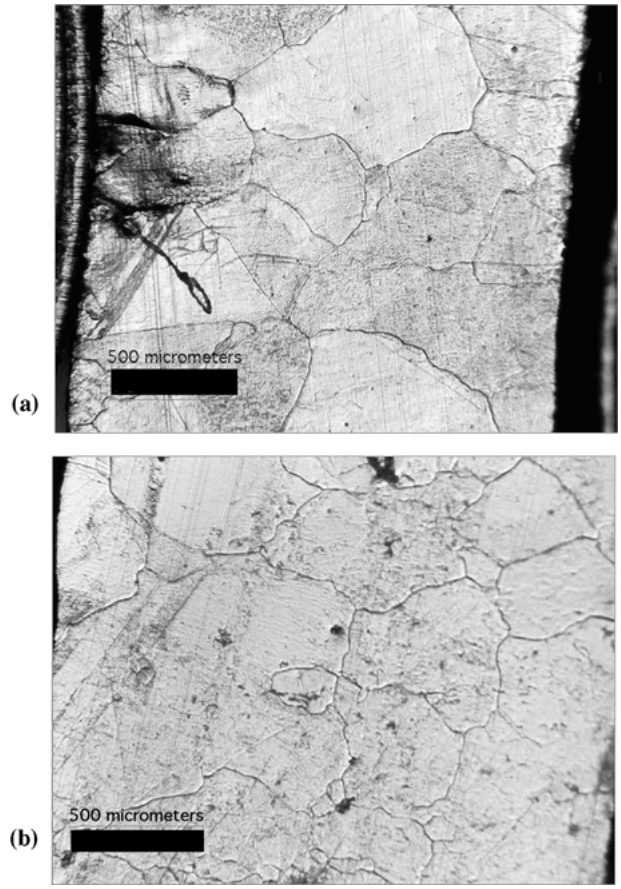

Figure 4 Reflected-light micrographs of microtomed-and-etched β-In_3Sn specimens; the microscopy specimens were prepared subsequent to the oscillatory damping testing. (a) Cast + pressed + annealed (389K; 3.5 h) specimen. (b) Cast + pressed + annealed + crept ($[\sigma_1 - \sigma_3] = 2.04$ MPa; $\varepsilon = 0.3$) specimen. Distinctly obvious in the crept specimen (b) are the ubiquitous serrations of the grain boundaries, indicating both dislocation flow and significant grain-boundary-migration recrystallization accompanying the creep. Nevertheless, the crept specimen reveals less damping than does the annealed material (cf. Fig. 3).

eutectic (52 at.% Sn, 48 at.% In) [25]. Observe that the slope of the tan δ curve for β is less than that of the eutectic and of γ from 0.01 Hz to 10 Hz. For cast β, the shear and Young's moduli were $G = 5.1$ GPa and $E = 15.9$ GPa, respectively, at 10 Hz. By comparison, for the eutectic, $G = 7.5$ GPa at 100 Hz; for pure In, $G = 4.1$ GPa at 100 Hz and for pure Sn, $G = 15.7$ GPa at 100 Hz. In β, there appears to be a range of frequency in which tan δ vs. frequency has a small, near zero slope. β-γ eutectic tan δ behavior lies between that of β and γ above about 2 Hz; tan δ for β crosses over that of the eutectic near 1 Hz.

The trends seen in the torsion study for single-phase β, with the varied methods of specimen preparation, are shown in Fig. 3. On an expanded scale, some differences are visible. While at frequencies below $\sim$1 Hz, none of the results differ by more than 10% (such small differences are usually not consequential since they can arise from specimen-to-specimen variations or from error), at higher frequencies the different preparation methods reveal significant effects on tan δ. Specifically, one sees that tan δ decreases going from cast to cast + annealed to cast + annealed + crept. Comparing the crept specimens (e.g., at $\sim$10 Hz) sees significant differences, too: the specimen crept at a differential stress of 1.35 MPa had a lower tan δ than the one crept at 2.04 MPa. Of note, too, is the emergence of an absorption (Debye) peak near 10^2 Hz, which is clearly imaged in the response of the crept specimens but is, nevertheless, visible in the pressed and pressed + annealed specimens. The first resonance occurred between 3800–5000 Hz for all specimens in torsion. Split-peaks at the first resonance appeared in torsion, preventing a determination of tan δ at that frequency, therefore such data were masked.

Microstructures of the as-cast and plastically deformed (pressed) specimens, obtained through optical microscopy, are shown in Fig. 4. Line-intercept analyses of the grain size revealed nominally equiaxed grains with a size 510 ± 73 μm for the as-cast material, 440 ± 77 μm for the pressed material, 760 ± 156 μm for the pressed and annealed material and 680 ± 95 μm and 640 ± 93 μm for the materials crept at 1.35 and 2 MPa, respectively. (Errors represent one standard deviation of the mean value for each of eight line scans per specimen.) Thus, the grain size is significant relative to the specimen size, i.e., there are but few grains in the cross section of any given test specimen. Also evident in the pressed and crept specimens are ubiquitous serrations in the grain boundaries, which are indicative of the mobility of the grain boundaries exceeding significantly that of the low-angle, subgrain boundaries for the thermodynamic conditions employed in the creep experiments.

4. Discussion

4.1. Damping behavior of single-phase β-In_3Sn

None of the arguments presented in the Introduction concerning the role(s) played by low- and high-angle boundaries in the mechanical absorption behavior leading to the power-law signature are invalidated by the present experimental results for damping in

single-phase β. At the same time, however, the results of the various processing steps (with the possible exception of annealing) to effect changes in the microstructure were minimal, due inevitably to the very high homologous temperature (room temperature, i.e., $T_h \approx 0.73 T_{solidus}$) at which the specimens were stored and tested.

Most clearly seen in Fig. 3, high-stress/high-rate deformation (pressing) increased tan δ while annealing significantly decreased damping. This behavior is anticipated, whether one envisions the damping arising from the oscillatory motion of numerous, weakly interacting (i.e., nominally mobile), variably (i.e., by length) pinned lattice dislocations and/or the chemical-diffusion-based relaxation of ordered dislocation arrays. It is the response of the crept specimens, however, that supports uniquely, at least in part, the low-angle boundary-absorption model outlined in the Introduction. Given that the density of mobile dislocations (ρ) effecting steady-state creep is directly related to the differential stress ($\rho \propto [\sigma_1 - \sigma_3]^2$) [18], creep is clearly suggested to increase the damping over that of material that has been carefully annealed. The requirements to lower the dislocation-effected damping in materials deformed to significant strain in creep, then, are (a) to not have a significant damping effect of the mobile dislocations and (b) to lower significantly the variability of structures of low- and high-angle grain boundaries as a result of the creep. The latter is clearly the case here, affected (exaggerated), too, by the small number of grains in the specimen cross-section.

At the same time, this simplification of substructure allows examination of the low-angle boundary effect on damping described in the Introduction. The relaxation process associated with both low- and high-angle boundaries can be characterized by a characteristic time, τ, which, for the case where chemical diffusion is confined to the boundaries themselves, is given by [10, 12]:

$$\tau = \frac{3\sqrt{3}(1-\nu^2)\, d^3 kT}{2\pi^3 E D_b \xi \Omega} \tag{3}$$

where ν is Poisson's ratio, d is the (sub)grain size, D_b is the grain-boundary diffusion coefficient for the rate-limiting species, ξ is the characteristic grain boundary width, and Ω is the molecular volume. This τ is not to be confused with the standard period ascribed to an exponential decay process in a linearly viscoelastic solid, rather, it produces essentially the entire power-law damping curve: τ articulates the relaxation associated with chemical diffusion within a diminishing potential gradient; the strain rate decays to within 1% of the steady-state (i.e., as represented by the submicrostructure) value by $\sim 0.25\,\tau$. (Equation 3 represents a relaxation rate-limited by diffusion on the subgrain boundaries; if that limitation is by lattice diffusion, the subgrain size dependence goes as $\tau \propto d^2$.)

One can apply Equation 3 in two ways to the analysis of the shear damping behavior. Employing the (relatively temperature-insensitive) relationship between the spacing of subgrain boundaries and the magnitude of differential stress ($[d/b] \propto [(\sigma_1 - \sigma_3)/G]^{-1}$ [18], where b is the magnitude of the Burgers vector, which is 0.329 nm for 1/2 $[101]_{fct}$ in β), one estimates that the spacing is $d \approx 10.5\ \mu$m and $d \approx 6.7\ \mu$m for differential stresses of 1.35 and 2.04 MPa, respectively. The result indicates a shift in frequency ($f \propto 1/\tau$) for the absorption curves of approximately 0.5 log units, which is very close that observed in Fig. 3. Analysis beyond this, i.e., using Equation 3 to predict *a priori* the high-T background, requires knowledge of the appropriate diffusion coefficient and its temperature sensitivity, as well as the structural (i.e., diffusion) width of the low-angle boundaries. There are no direct data for grain boundary or dislocation "pipe" diffusion in β-In_3Sn, nor direct measurements of grain boundary structural width in this material. One can, however, use semi-empirical approaches to estimate the values for diffusion [30, 31] and, assuming a structural width for the low-angle boundaries of 1 nm [32], calculate a value of $(D_b \xi) = 2.4 \times 10^{-22}$ m^2 s^{-1} at room temperature; this estimate carries on to produce a value of $\tau = 875$ s for the specimen crept at $\sim$2 MPa prior to the oscillatory loading test. Behavior of the boundary-diffusion-based model for the high-T background predicts a tan δ of 10^{-2} at $f = 10^3/\tau$ [10]; one sees in Fig. 3, then, a distinctly reasonable agreement.

The effects of the creep treatment, specifically the strain-affected narrowing of the distribution of grain and subgrain boundary structures and the consequent lowering of the damping overall, suggests plainly that the crossing of the as-cast β-phase damping curve with that of the β-γ eutectic (Fig. 2) is created/caused by a broad peak associated with the discrete damping behavior of various structures (albeit a limited number, given the limited slip systems in β and the small number of grains in the specimen cross section) of grain boundaries. Similar behavior is seen in polycrystalline aluminum: fine random grain structures produce a broad swell (width approximately four orders of magnitude in frequency) above the high-T background [21] while low-angle boundaries in deformed and partially annealed (i.e., to effect formation of low-angle boundaries) specimens show a sharpening of peaks to a width less than two orders of magnitude in frequency [20]. This tendency is highlighted, too, in the present experiments: the data in Fig. 3 for the as-cast, pressed-and-annealed and pressed-annealed-and-crept specimens demonstrate the formation of a peak centered near $f = 10^2$ Hz, affected strongly by the creep treatment.

What is clear, however, is the strong impact of grain and, particularly, subgrain boundaries in effecting the high-T background. As such, one anticipates that phase boundaries, e.g., as expressed in eutectic structures, should have a powerful effect on damping, both in the absolute value of tan δ and in the power-law distribution characteristic of the high-T background.

4.2. β-γ Eutectic: The failure of simple composite theory and the importance of phase boundaries

Eutectic microstructures are frequently contemplated as a composite material. Such microstructure can be a complex assemblage of laminae, difficult to study

via exact analytical solutions. Nevertheless, composite theory offers bounds on the behavior of arbitrarily complex structure. The upper and lower bounds on the elastic moduli of an *isotropic* composite as a function of volume fraction are known. The lower bound for the elastic shear modulus, G_L of the composite is given as [33]:

$$G_L = G_2 + \frac{V_1}{\frac{1}{G_1 - G_2} + \frac{6(K_2+2G_2)V_2}{5(3K_2+4G_2)G_2}}, \quad (4)$$

in which K_1, G_1 and V_1 and K_2, G_2 and V_2 the bulk modulus, shear modulus and volume fraction of phases 1, and 2, respectively. Here $G_1 > G_2$ so that G_L represents the lower bound on the shear modulus. Interchanging the numbers 1 and 2 in Equation 4 results in the upper bound G_U for the shear modulus. For viscoelastic materials, the correspondence principle is applied [34]; the complex viscoelastic shear moduli of the composite G_L^* and G_U^* are:

$$G_L^* = G_2^* + \frac{V_1}{\frac{1}{G_1^* - G_2^*} + \frac{6(K_2^*+2G_2^*)V_2}{5(3K_2^*+4G_2^*)G_2^*}}, \quad \text{and} \quad (5)$$

$$G_U^* = G_1^* + \frac{V_2}{\frac{1}{G_2^* - G_1^*} + \frac{6(K_1^*+2G_1^*)V_1}{5(3K_1^*+4G_1^*)G_1^*}}. \quad (6)$$

In these cases the loss tangent is complicated to write explicitly, so it is expedient to obtain it by computation. The Hashin-Shtrikman formulae are not bounds for the viscoelastic behavior, but they are close to the bounds [35, 36] and for some microstructures they coincide with the bounds.

The dynamic response of β-γ eutectic was contemplated in the context of composite theory (cf. [37]). Incompatibility with the bounds is indicated by differences in the shape of the curves of damping vs. frequency for the component phases and the eutectic. The present results (Fig. 2) show damping of β-In_3Sn crosses over that of the eutectic. Such behavior is manifestly inconsistent with the composite bounds, in which tan δ of a composite must lie between that of the constituents. Therefore the eutectic cannot be simply a mechanical composite of the β and γ phases. Consistent fully with the results for single-phase β presented here, it is likely that interfaces play a role not anticipated in the elementary composite theory, which assumes a purely rigid interface.

In the β-γ eutectic, rolling (high-stress/high-strain-rate shear deformation) introduces a significant increase in phase-boundary density by finely dividing the more brittle γ phase (cf. [38]); the result is significantly increased damping at fixed frequency (Fig. 5)—damping distinctly greater than that seen for the pressing processing of the single-phase β (cf. Fig. 3). The result can perhaps be interpreted as a greater "potency" for mechanical absorption of phase boundaries than for low- or high-angle boundaries in single-phase aggregates (cf. the proposal relating superplasticity and superanelasticity in Pb-Sn eutectic [39] as well as the absorption response of superplastic eutectoid Al–Zn [40]). We believe a better interpretation of the effect

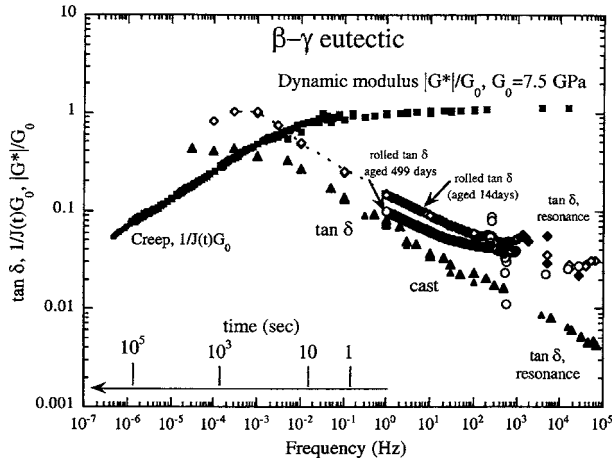

Figure 5 Room-temperature, torsional viscoelastic response (tan δ) as a function of frequency for the β-γ eutectic in the as-cast condition as well as subsequent (1) to rolling and (2) room-temperature aging for significant time. The rolling processing, by finely dividing and dispersing the more-brittle γ phase, produces significantly greater damping, pointing strongly to the role of phase boundaries in the absorption response. That the aging affects the damping non-uniformly indicates that the loss in damping is not simply related to microstructural coarsening, but involves preferential loss of certain phase boundary structures.

is a change in τ (Equation 3), which shifts the damping band to higher frequency as the effective boundary viscosity drops for a fixed grain size. Boundary viscosity is first-order affected by the dislocation structure of the boundary (cf. [41]); the boundary viscosity should drop as crystalline symmetry elements are lost/changed across the boundary—clearly the case for a phase boundary.

Fig. 5 additionally presents the results of long-term thermal aging on the absorption of the rolled β-γ eutectic. One sees that the thermal evolution of the microstructure does not simply shift the entire absorption curve to lower frequencies, which would be expected (cf. Equation 3) if the aging were simply an Ostwald ripening (coarsening) of the dispersed γ phase in the eutectic. Rather, one discovers a lowering of tan δ for the lower frequencies tested ($\sim$1 Hz) but a retention of the rolling-effected, enhanced absorption at high frequency. This is a behavior suggestive of a loss, via the thermal aging, of only certain phase boundary structures: thermal energy will allow relaxation of phase boundary structure such that (via faceting, for example) lower-elastic-energy morphologies occur (cf. [42]). As such, the result is effectively compared to the impact of creep on the absorption in single-phase β (cf. Fig. and the discussion in Section 4.1).

5. Summary and conclusions

The torsional damping behavior of single phase β-In_3Sn has been evaluated over a broad frequency range and as a function of various mechanical and thermal treatments. The results are consistent—albeit, perhaps, not uniquely—with a model for the power-law (tan $\delta \propto f^{-n}$, $0.2 \leq n \leq 0.4$), high-T background absorption being effected by diffusional processes on grain and subgrain boundaries. Strong evidence for the domination of boundaries is that creep to high strain

effects a significant *reduction* in damping for certain frequencies. The results are compared/contrasted with those for damping in single-phase γ-$InSn_4$ and in the two-phase β-γ eutectic. Failure of the eutectic material to follow a composite model for damping, combined with a thermal aging effect that lowers damping only for certain frequencies, shows that the boundary-based absorption model applies, too, to phase boundaries.

Acknowledgments

We thank Mark Ludwigson for preparing the β samples; we thank, too, Joe Bunton for his advice and assistance in all areas of microstructural specimen preparation and analysis. The microtome is housed in the UW–Madison Integrated Microscopy Center; Randy Massey provided both access and assistance. This work was financially supported, in part, by grants from the National Science Foundation (CMS-9896284 to RSL and EAR-0106620 to RFC).

References

1. J. ZHANG, R. J. PEREZ and C. R. WONG, *Mater. Sci. Engr.* **13** (1994) 325.
2. J. ZHANG, R. J. PEREZ and E. J. LAVERNIA, *J. Mater. Sci.* **28** (1993) 835.
3. M. BRODT and R. S. LAKES, *J. Composite Mater.* **29** (1995) 1823.
4. R. S. LAKES and J. QUACKENBUSH, *Philos. Mag. Lett.* **74** (1996) 227.
5. J. E. BISHOP and V. K. KINRA, *Mech. Composite Mater. Struct.* **1** (1994) 75.
6. C. ZENER, "Elasticity and Anelasticity of Metals" (Univ. of Chicago Press, Chicago, 1948).
7. A. S. NOWICK and B. S. BERRY, "Anelastic Relaxation in Crystalline Solids" (Academic Press, New York, 1972).
8. G. SCHOECK, E. BISOGNI and J. SHYNE, *Acta Metall.* **12** (1964) 1466.
9. W. N. FINDLEY, J. S. LAI and K. ONARAN, "Creep and Relaxation of Nonlinear Viscoelastic Materials" (North-Holland, New York, 1976).
10. T. T. GRIBB and R. F. COOPER, *J. Geophys. Res.* **103** (1998) 27267.
11. E. N. DaC. ANDRADE, *Proc. R. Soc. London* **A84** (1910) 1.
12. R. RAJ, *Metall. Trans. A* **6A** (1975) 1499.
13. F. R. N. NABARRO, in "Report of a Conference on the Strength of Solids" (Phys. Soc. London, 1948) p. 75.
14. C. HERRING, *J. Appl. Phys.* **21** (1950) 437.
15. R. L. COBLE, *ibid.* **34** (1963) 1679.
16. Y. GUEGUEN, M. DAROT and P. MAZOT, *Phys. Earth Planet. Inter.* **55** (1989) 254.
17. G. GLOVER and C. M. SELLARS, *Metall. Trans.* **4** (1973) 765.
18. R. J. TWISS, *Pure Appl. Geophys.* **115** (1977) 227.
19. T. S. KÊ, *Phys. Rev.* **71** (1947) 533.
20. S. C. YAN and T. S. KÊ, *Phys. Stat. Solidi* **104** (1987) 715.
21. A. RIVIÈRE and P. GADAUD, *Metall. Mater. Trans. A* **28A** (1997) 1661.
22. Q. P. KONG, B. CAI and G. GOTTSTEIN, *J. Mater. Sci.* **36** (2001) 5429.
23. R. RAJ and M. F. ASHBY, *Metall. Trans.* **2** (1971) 1113.
24. D. S. STONE, *Acta Metall. Mater.* **39** (1991) 599.
25. R. HULTGREN, P. D. DESAI and D. T. HAWKINS, "Selected Values of the Thermodynamic Properties of Binary Alloys" (American Society for Metals, Metals Park, OH, 1973).
26. M. BRODT, L. S. COOK and R. S. LAKES, *Rev. Sci. Instr.* **66** (1995) 5292.
27. C. P. CHEN and R. S. LAKES, *J. Rheol.* **33** (1989) 1231.
28. W. DUFFY, *J. Appl. Phys.* **68** (1990) 5601.
29. P. M. BUECHNER, D. S. STONE and R. S. LAKES, *Scripta Mater.* **41** (1999) 561.
30. R. J. BORG and G. J. DIENES, "An Introduction to Solid-State Diffusion" (Academic, Boston, 1988) p. 80.
31. H. J. FROST and M. F. ASHBY, "Deformation Mechanism Maps: The Plasticity and Creep of Metals and Ceramics" (Pergamon, Oxford, UK, 1982) p. 32.
32. A. KELLY and G. W. GROVES, "Crystallography and Crystal Defects" (Addison-Wesley, Reading, PA, 1970) p. 345.
33. Z. HASHIN and S. SHTRIKMAN, *J. Mech. Phys. Solids* **11** (1963) 127.
34. R. M. CHRISTENSEN, *ibid.* **17** (1969) 23.
35. L. V. GIBIANSKY and G. W. MILTON, *Proc. R. Soc. London* **440** (1993) 163.
36. L. GIBIANSKY and R. S. LAKES, *Mech. Mater.* **16** (1993) 317.
37. M. BRODT and R. S. LAKES, *J. Mater. Sci.* **31** (1996) 6577.
38. J. W. MORRIS JR., J. L. FREER-GOLDSTEIN and Z. MEI, *J. Metals* **45** (1993) 25.
39. J. H. SCHNEIBEL and P. M. HAZZLEDINE, *Acta Metall.* **30** (1982) 1223.
40. J. LU and D. C. VAN AKEN, *Metall. Mater. Trans. A* **27A** (1996) 2565.
41. M. F. ASHBY, *Surface Sci.* **31**(1972) 498.
42. P. H. PUMPHREY, in "Grain Boundary Structure and Properties", edited by G. A. Chadwick and D. A. Smith (Academic, London, 1976) ch. 5.

Received 30 January 2002
and accepted 5 March 2003